Modeling snow saltation: the effect of grain size and interparticle cohesion

Daniela Brito Melo[1], Varun Sharma[2], Francesco Comola[3], Armin Sigmund[1], and Michael Lehning[4]

[1]Ecole Polytechnique Fédérale de Lausanne
[2]École Polytechnique Fédérale de Lausanne
[3]University of California, Los Angeles
[4]EPFL and SLF Davos

November 22, 2022

Abstract

The surface of the Earth is snow-covered at least seasonally over large areas. This snow surface is highly dynamic, particularly under the influence of strong winds. The motion of snow particles driven by the wind not only changes the snow cover but has important consequences for the atmosphere in that it adds mass and moisture and extracts heat. Large scale meteorological and climatological models neglect these surface dynamics or produce conflicting results from too simplified process representation. With recent progress in the detailed understanding of the saltation process, in particular with respect to sand saltation, and the advancement of numerical models, we can systematically investigate the influence of snow properties on saltation. This contribution uses a Large Eddy Simulation (LES) model with full surface particle dynamics to investigate how snow cohesion and size distribution influence saltation dynamics and in particular the total mass flux. The model reproduces some known characteristics of the saltation system such as a focus point or a constant near surface particle speed. An interesting result is that cohesion and grain size heterogeneity can increase the overall saltation mass flux at high friction velocities. Moreover, some simplified models agree reasonably well with the simulations for given bed characteristics, while others clearly do not. These results are valid for continuous saltation while intermittent saltation, which often occurs in nature, needs further investigation. In order to successfully parameterize saltation in large scale models, progress must be made in correctly representing snow surface properties in these models, in particular cohesion.

Modeling snow saltation: the effect of grain size and interparticle cohesion

D. B. Melo[1], V. Sharma[1], F. Comola[2], A. Sigmund[1], M. Lehning[1,3]

[1]School of Architecture, Civil and Environmental Engineering, Ecole Polytechnique Fédérale de Lausanne, Lausanne, Switzerland
[2]Department of Atmospheric and Oceanic Sciences, University of California, Los Angeles, USA
[3]WSL Institute of Snow and Avalanche Research SLF, Davos, Switzerland

Key Points:

- The numerical model employed is able to simulate the main steady state saltation characteristics
- Cohesion and grain size heterogeneity increase snow saltation mass flux at high friction velocities
- Improved estimates of snow saltation mass flux must take into account the bed properties

Corresponding author: D. B. Melo, daniela.britomelo@epfl.ch

Abstract

The surface of the Earth is snow-covered at least seasonally over large areas. This snow surface is highly dynamic, particularly under the influence of strong winds. The motion of snow particles driven by the wind not only changes the snow cover but has important consequences for the atmosphere in that it adds mass and moisture and extracts heat. Large scale meteorological and climatological models neglect these surface dynamics or produce conflicting results from too simplified process representation. With recent progress in the detailed understanding of the saltation process, in particular with respect to sand saltation, and the advancement of numerical models, we can systematically investigate the influence of snow properties on saltation. This contribution uses a Large Eddy Simulation (LES) model with full surface particle dynamics to investigate how snow cohesion and size distribution influence saltation dynamics and in particular the total mass flux. The model reproduces some known characteristics of the saltation system such as a focus point or a constant near surface particle speed. An interesting result is that cohesion and grain size heterogeneity can increase the overall saltation mass flux at high friction velocities. Moreover, some simplified models agree reasonably well with the simulations for given bed characteristics, while others clearly do not. These results are valid for continuous saltation while intermittent saltation, which often occurs in nature, needs further investigation. In order to successfully parameterize saltation in large scale models, progress must be made in correctly representing snow surface properties in these models, in particular cohesion.

1 Introduction

Wind erosion of snow covered surfaces is frequently observed in alpine and polar regions. Snow transport leads to the formation of bedforms, intensifies snow sublimation and modifies the microstructure of surface snow layers. Moreover, the interaction between the wind field and the complex topography creates regions of enhanced snow erosion and deposition, which greatly contributes to snow height heterogeneity. In alpine regions, these processes are of great importance for water management and avalanche risk assessment (Lehning et al., 2008). In Antarctica, snow transport is enhanced by the katabatic winds, dominating large areas from the inner plateau to the coast, and clouds of blowing snow particles with a height of hundreds of meters can be observed (Palm et al., 2017).

The aeolian transport of snow occurs at different heights above the ground. The terms drifting snow and blowing snow are commonly used to indicate, respectively, the movement of snow particles close to the surface (up to approximately 2 m height) and the movement of smaller snow particles transported at high elevations. In the first 10 cm above the surface, snow particles are mainly transported in saltation (Bagnold, 1941): they follow short ballistic trajectories and generally hit the ground with enough kinetic energy to hop again (rebound) or eject other particles on the bed (splash). Above the saltation layer, given by the ensemble of saltating particles, smaller grains are transported in suspension: they mainly follow the wind flow and travel great distances before being deposited on the ground or sublimate.

At low wind speeds, the mass flux in saltation is greater than the mass flux of suspended particles. At high wind speeds, snow transport in suspension becomes relevant and is currently simulated in mesoscale models by advection-diffusion equations (Lehning et al., 2008; Lenaerts et al., 2012; Vionnet et al., 2014; Amory et al., 2015). Particle concentration in the saltation layer defines the lower boundary condition for snow suspension. The saltation models commonly used in these mesoscale models rely on simple analytical equations based on the assumption of steady state saltation, that is, an equilibrium state between the grains in motion and the wind field (Pomeroy & Gray, 1990; Doorschot & Lehning, 2002; Sørensen, 2004). However, the parameters used in the referred analytical saltation models are highly uncertain and do not always reflect the properties of the snow type. This limits the accuracy of the mass flux of particles in suspension, which is either underestimated (Amory et al., 2015) or overestimated (Vionnet et al., 2014). As a consequence, uncertainties arise in the rate of blowing snow sublimation and the consequent increase in the atmospheric moisture content. For instance, snow sublimation is the main mass-depleting process in some regions of the Antarctic ice sheet, but the contribution of blowing snow sublimation is still largely unknown (Van Wessem et al., 2018; Agosta et al., 2019). Hence, even though snow saltation is usually a sub-grid process in mesoscale models, its correct modeling greatly influences the mass and energy balances at a larger scale.

The complexity of modeling snow saltation is related to the turbulent flow features and the snow particle characteristics. In contrast with sand beds, snow beds change continuously: soon after deposition, snow grains form interparticle ice bonds between each other; the characteristics of a snow bed (for instance, particle size distribution, interparticle bonds and grain shape) evolve with time due to metamorphic processes; and snow particle sizes change during saltation events due to fragmentation (Comola et al., 2017) and sublimation (Sharma et al., 2018).

Detailed models of saltation are ideal to simulate both the flow and snow bed particularities. By explicitly solving the turbulent flow, particle trajectories and the surface processes, these models can be used to improve our understanding of particle-wind interaction and to evaluate some of the assumptions made in simple saltation models. In the last two decades, Reynolds-Averaged Navier-Stokes (RANS) and Large Eddy Simulation (LES) flow solver techniques were used, coupled with Lagrangian models for particle dynamics (e.g., Shao & Li, 1999; Almeida et al., 2006; Dupont et al., 2013; Groot Zwaaftink et al., 2014; Okaze et al., 2018). Moreover, splash laws based on conservation principles were also proposed and used to describe steady state saltation (Kok & Renno, 2009; Lämmel et al., 2017; Comola & Lehning, 2017).

Recent theoretical and numerical advances (Comola & Lehning, 2017; Comola, Gaume, et al., 2019) have shed light into the role played by granular bed properties, such as grain size distribution and interparticle cohesion, in granular splash mechanisms. In addition, field measurements of sand saltation (Martin & Kok, 2019) have questioned the idea of modeling each grain size bin independently when assessing saltation onset over mixed-sized beds. However, the effect of snow surface properties on saltation development and scaling laws is still largely unknown. For example, there are no estimates on how particle size distribution and interparticle cohesion influence particle speed and surface friction velocity during saltation. Consequently, the effect of surface properties on the integrated mass flux is still unclear.

In this work, we use an LES solver coupled with a Lagrangian model to compute particle-wind interactions (Comola, 2017) and the splash functions proposed by Comola and Lehning (2017) to describe particle-bed interactions. The capabilities of this model to simulate steady state saltation are firstly assessed. The vertical profiles of wind speed, saltation mass flux, concentration and particle velocity are analyzed, as well as the variation of the integrated mass flux with the friction velocity. Then, a detailed study on the effect of grain size and interparticle cohesion on the vertical profiles, integrated mass flux and surface friction velocity is performed. To this end, the properties of the granular bed are varied in a systematic way in a suite of simulations, which cover a range of wind velocities. The results are compared to existing saltation models and to the conclusions drawn from the latest wind tunnel and field experiments.

This article shows the potential of LES-based models coupled with state-of-the-art splash functions to simulate steady state saltation and to improve our understanding of saltation dynamics. Moreover, it sheds light onto the relative importance of grain size and interparticle cohesion for snow saltation characteristics. The work presented ultimately helps progressing towards the development of new saltation mass flux parameterizations, which would take into account the influence of surface snow properties.

The model details are presented in section 2. In section 3, the numerical setup used for the simulations is presented. The results are shown and discussed in section 4 and the main conclusions are summarized in section 5.

2 Flow and particle dynamics

2.1 Flow solver

The tri-dimensional wind field is solved with the Large Eddy Simulation (LES) technique. Turbulence features larger than the grid size are resolved by the filtered continuity and Navier-Stokes equations, while the effect of smaller eddies is parameterized by a sub-grid scale (SGS) model. The LES model used along with the particles solver is named EPFL-LES. It was developed at the Ecole Polytechnique Fédérale de Lausanne and is based on the work of Albertson and Parlange (1999).

The LES code targets atmospheric boundary layer (ABL) flows, assumed incompressible and driven by a constant streamwise pressure gradient, $\partial p_\infty/\partial x$:

$$\frac{\partial p_\infty}{\partial x} = -\rho_f \frac{u_*^2}{L_z} \tag{1}$$

where ρ_f is the fluid density, L_z is the domain height and u_* is the desired friction velocity.

Horizontal gradients are computed with a Fourier-based pseudo-spectral approach and vertical gradients are calculated using second-order finite differences. The time derivatives are computed with the second-order Adams-Bashforth time advancement scheme (Canuto et al., 1988). In the present code version, the closure SGS model is given by the scale-dependent Lagrangian dynamic model (LASD) as proposed by Bou-Zeid et al. (2005). This model exhibits better dissipation characteristics than the classic Smagorinsky and the scale-invariant dynamic models.

Periodic boundary conditions are imposed in the vertical walls of the computational domain, as required when applying Fourier transforms, allowing for the development of a fully turbulent flow at both the inlet and outlet sections. At the top boundary, impermeability and zero vertical gradients are assumed. At the bottom boundary, the impermeability condition is imposed and the wall shear stress is given by the logarithmic law of the wall. The use of wall functions avoids highly discretized meshes near the surface as well as smaller time steps to guarantee numerical stability.

The present LES code has been used in multiple ABL studies concerning land-atmosphere interaction over complex terrains, wind-farms and urban canopy (Albertson & Parlange, 1999; Bou-Zeid et al., 2005; Diebold et al., 2013; Giometto et al., 2016, 2017; Sharma et al., 2017). A detailed description of the model can be found in these works.

2.2 Particle dynamics

Particle motion is computed in a Lagrangian framework. The coupling with the LES solver was developed by Comola (2017), following the work of Groot Zwaaftink et al. (2014). The model has been further developed with the contributions of Comola and Lehning (2017), Sharma et al. (2018) and Comola, Giometto, et al. (2019).

Particle inertia, gravity and aerodynamic drag are related by Newton's second law. Aerodynamic drag, D_i, is given by $D_i = -1/2 C_D \rho_f A_f \, |U_r| \, U_{r,i}$, where $i = 1, 2, 3$ denotes the x (streamwise), y (crosswise) and z (vertical) directions in the Cartesian coordinate system. C_D is the drag coefficient, A_f is the particle frontal area, $U_{r,i}$ the particle velocity relative to the local flow and $|U_r|$ its absolute value (henceforth referred to as U_r). In the current model, saltating particles are assumed spherical, with a frontal area $A_f = \pi d^2/4$, where d is the particle diameter. The drag coefficient is estimated using the expression proposed by Schiller and Nauman (Clift et al., 1978) as a function of the particle Reynolds number, $Re_d = U_r d/\nu_f$, where ν_f is the fluid kinematic viscosity:

$$C_D = \frac{24}{Re_d}\left(1 + 0.15 Re_d^{0.687}\right). \tag{2}$$

The equation for particle trajectory yields:

$$du_{p,i} = \left[\frac{3}{4}\frac{\rho_f}{\rho_p}\frac{C_D}{d}U_r\left(u_i - u_{p,i}\right) - g\delta_{i3}\right]dt \tag{3}$$

where $u_{p,i}$ is the particle velocity, u_i is the instantaneous flow velocity resolved by the LES solver, ρ_p is the particle density, g is the acceleration of gravity, t is the time variable and δ is the Kronecker delta. Equation 3 is solved numerically with a first-order forward Euler method.

Other forces such as aerodynamic lift, electrostatic forces and those from interparticle collision are expected to be smaller than weight and drag and are generally neglected when modeling saltation in air (Maxey & Riley, 1983; Anderson & Hallet, 1986). Their effect on sand saltation was studied by several authors (e.g., D. S. Schmidt et al., 1998; Kok & Renno, 2006, 2008; Huang et al., 2007; Durán et al., 2011) and further investigation is needed to fully assess their impact on particle trajectory (Kok et al., 2012). Moreover, snow sublimation is not taken into account.

In previous works based on this model (Groot Zwaaftink et al., 2014; Sharma et al., 2018; Comola, Giometto, et al., 2019), the non-resolved SGS velocities were computed. Then, the instantaneous wind field was derived from the sum of the resolved wind velocity field, u_i, and the SGS velocities. The modeling of velocity fluctuations is important when using simple flow models, as COMSALT (Kok & Renno, 2009), or RANS solvers (Nemoto & Nishimura, 2004). In these models, turbulence is not resolved and a model for high-frequency velocity fluctuations is imperative. However, the importance of such a model is less clear for LES, as the large scale instantaneous turbulent flow is provided as a solution of the flow solver. In fact, Dupont et al. (2013) concluded that the SGS velocities have a negligible effect on particle trajectories. Moreover, Z. Wang et al. (2019) did not consider the SGS velocities when modeling saltation with an LES solver. The impact of SGS velocities on particle trajectories may also depend on the SGS model employed, even though there are no works in the literature regarding this question. In this work, the effect of the SGS turbulence features on the resolved wind velocity field is modeled with one of the most advanced SGS closure schemes, the LASD (Bou-Zeid et al., 2005). Thus, the effect of the SGS velocities on particle motion is assumed to be negligible and not taken into account.

The feedback of particle motion on flow momentum is modelled through a source term, S_i, in the Navier-Stokes equations. S_i is given by the total drag force induced by the particles, corresponding to the sum of $-D_i$, per unit volume. The contribution of each particle is linearly extrapolated to the nearest eight grid nodes where LES is resolved.

Periodic boundary conditions are applied to particles exiting the domain through its vertical walls. Particles that reach the top boundary are assumed to leave the domain and those impacting the bottom boundary (erodible bed) may rebound and eject other grains as described in section 2.3.

Different studies have been conducted with previous and current versions of this model concerning snow saltation variability (Groot Zwaaftink et al., 2014), drifting snow sublimation (Sharma et al., 2018) and preferential deposition over hills (Comola, Giometto, et al., 2019). A detailed description of the model algorithm and a comparison between simulation results and field/wind tunnel measurements can be found in these works.

2.3 Surface processes

The interaction between surface grains, the wind flow and particles impacting the bed is described by three main processes: aerodynamic entrainment, rebound and splash. These surface processes are modelled with statistical models based on physical principles and experimental correlations, as proposed by Groot Zwaaftink et al. (2014) and further developed by Comola and Lehning (2017).

This approach reduces the computational cost associated with the direct numerical simulation of particle interactions within the granular bed. Saltation models based on the Discrete Element Method (DEM) simulate these complex interactions, but are not suitable for simulating particle transport over large computational domains (Durán et al., 2012; Pähtz et al., 2015; Comola, Gaume, et al., 2019).

2.3.1 Aerodynamic entrainment

When a fluid flows over a granular and erodible bed, surface particles can be moved and eventually lifted by the flow. This process is called aerodynamic entrainment and occurs when the fluid surface shear stress grows above a given threshold. This threshold, that defines the start of wind erosion, is estimated by considering the forces applied on a grain laying on the bed and by performing a balance of angular momentum. The quantity of interest is the minimum aerodynamic force that makes the grain rotate over its leeward point of contact with the underlying grains and, eventually, leads to an uplift of the grain.

In general, this threshold shear stress is modeled as a mean quantity, related to the instantaneous aerodynamic force by a parameterization. Bagnold (1941) named it the fluid threshold, τ_{ft}. Considering particle weight, buoyancy and drag, he proposed the following well known expression:

$$\tau_{ft} = A^2 \left(\rho_p - \rho_f\right) g d \tag{4}$$

where A is the fluid threshold coefficient, which depends on different flow and particle characteristics. Chepil (1959) deduced an expression for A, function of the turbulence intensity, particle geometry and drag coefficient, estimated by a series of experiments developed with sand and soil grains. Bagnold (1941) proposed $A = 0.1$ for sand beds, after a series of wind tunnel and field experiments. A higher value is expected for very small particles like dust. In this case, the granular surface is not aerodynamically rough and a thin viscous sub-layer is present close to the surface, which limits the transport of flow momentum to the bed. Different criteria have been proposed to define the onset of aerodynamic entrainment. A summary of the latest developments can be found in Pähtz et al. (2020).

Interparticle forces, as the van der Waals and electrostatic forces and those induced by interparticle bonds, also play a role in the aerodynamic entrainment of cohesive materials as snow or moist soils (R. A. Schmidt, 1980; Shao & Lu, 2000). However, the quantification of such forces is still a challenge. The contribution of interparticle ice bonds in the calculation of the fluid threshold is of special interest when studying the erosion of snow covered surfaces and was firstly addressed by R. A. Schmidt (1980). However, for common interparticle bond radius, the values estimated for τ_{ft} were too large for pure aerodynamic entrainment of snow particles to occur. Other authors as Lehning et al. (2000) and Clifton et al. (2006) used the same approach suggested by R. A. Schmidt (1980), but adjusted the bond properties and empirical constants to improve the agreement with wind tunnel tests performed with natural snow beds. The values for τ_{ft} obtained during wind tunnel and field experiments are lower than those deduced by R. A. Schmidt (1980), possibly because patches of loose snow grains are always present over dry snow surfaces. These grains can be easily lifted by the flow and contribute to the development of saltation by further ejecting other particles. Moreover, bed microtopography can also induce local peaks in shear stress, leading to the preferential entrainment of grains more exposed to the airflow.

In light of the challenges and uncertainties to correctly quantify the effect of interparticle forces on the fluid threshold, these forces are not taken into account in this work. Hence, τ_{ft} is computed from equation 4, considering the grain mean diameter, $\langle d \rangle$. This is a simpler approach suitable to study steady state saltation, where the contribution of aerodynamic entrainment is expected to be negligible (Kok et al., 2012).

The number of grains entrained per unit area per unit time, defined as the aerodynamic entrainment rate, N_{ae}, is computed by the expression proposed by Anderson and Haff (1991):

$$N_{ae} = \eta \left(\tau_s - \tau_{ft} \right) \tag{5}$$

where η is the entrainment coefficient and τ_s is the surface shear stress. τ_s is related to the surface friction velocity, $u_{*,s}$, by its definition: $\tau_s = \rho_f u_{*,s}^2$. Similarly, we introduce the fluid threshold friction velocity, $u_{*,ft}$, related to the fluid threshold shear stress by $\tau_{ft} = \rho_f u_{*,ft}^2$. The surface friction velocity differs from the imposed friction velocity, u_*, after saltation onset and the consequent exchange of momentum from the fluid to the particles. η is computed with the expression proposed by Doorschot and Lehning (2002):

$$\eta = \frac{C_{ae}}{8\pi \langle d \rangle^2} \tag{6}$$

where the coefficient C_{ae} is set to 1.5 grains m^2 N^{-1} s^{-1} (Groot Zwaaftink et al., 2014).

In the model, entrained particles start their trajectory at a height of four times the mean grain diameter. The initial velocity and vertical angle of ejection are defined according to a lognormal distribution as described in Clifton and Lehning (2008). The mean and standard deviation of the distribution are computed with the expressions presented in Table 1. The horizontal angle of ejection is given by the horizontal flow direction.

2.3.2 Rebound

After impacting the surface, a grain may rebound and eject other particles laying on the bed. The probability of rebound, P_r, is described by the expression proposed by Anderson and Haff (1991):

$$P_r = P_m \left[1 - \exp\left(-\gamma |u_{p,I}| \right) \right] \tag{7}$$

where P_m is the maximum probability of rebound, equal to 0.9 as proposed by Groot Zwaaftink et al. (2014) for snow particles, γ is a constant set to 2 s m^{-1} (Anderson & Haff, 1991) and $|u_{p,I}|$ is the particle velocity at impact.

The velocity of rebound, $|u_{p,R}|$, is given by $|u_{p,R}| = \sqrt{\epsilon_r} |u_{p,I}|$, where ϵ_r is the fraction of kinetic energy retained by the rebounding grain (restitution coefficient). Salta-

Table 1. Initial velocity of aerodynamically entrained, splashed and rebounding grains: distribution type, mean and standard deviation.

	Distribution	Mean	Std.	References
Aerodynamic entrainment				
Velocity magnitude	Lognormal	$3.5u_*$	$2.5u_*$	Clifton and Lehning (2008)
Vertical angle	Lognormal	$75 - 55\left[1 - \exp\left(-\frac{d}{175\times10^{-6}}\right)\right]$	15	Clifton and Lehning (2008)
Rebound				
Velocity magnitude	-	$\sqrt{\epsilon_r}\,\lvert u_{p,I}\rvert$	-	Kok and Renno (2009)
Vertical angle	Exponential	45	-	Kok and Renno (2009)
Splash				
Velocity magnitude	Exponential	$0.25\,\lvert u_{p,I}\rvert^{0.3}$	-	Sharma et al. (2018)
Vertical angle	Exponential	50	-	Rice et al. (1995, 1996)
Horizontal angle	Normal	Angle of impacting particle	15	Xing and He (2013)

Velocities are in units of m s^{-1}, angles are in degrees and the grain size is in meters.

tion models have shown to be highly sensitive to the value of ϵ_r, which greatly depends on the particle elastic properties (Kok & Renno, 2009). Experiments developed with sand showed that ϵ_r varies according to a normal distribution (D. Wang et al., 2008). Although the restitution coefficient for snow particles is more uncertain, experiments have not suggested a significant deviation from the values obtained for sand grains (Nalpanis et al., 1993).

The horizontal angle of rebound is given by the horizontal flow direction and the vertical angle is computed from an exponential distribution. Further details are presented in Table 1.

2.3.3 Splash

When a grain impacts the bed, it can eject several grains initially at rest. This process, named splash or ejection, is the main driver of particle motion during steady state saltation (Kok et al., 2012). As flow momentum decreases near the surface due to particle drag, aerodynamic entrainment is highly compromised after the start of saltation. Particles impacting the ground become the main source of momentum as they travel from high momentum regions to the surface.

Numerous statistical splash functions have been proposed to estimate the number of ejected grains, N, and their initial velocity, $|u_{p,o}|$, as a function of the impacting grain velocity, $|u_{p,I}|$, and mass, m_I (e.g., Anderson & Haff, 1988; McEwan & Willetts, 1991). In this work, the number of ejected grains is computed from energy and momentum conservation laws, as proposed by Kok and Renno (2009) and adapted by Comola and Lehning (2017) to take into account the effect of mixed-sized grains and interparticle cohesion.

The impacting grain and the bed are regarded as an isolated system, for which energy and momentum conservation is applied. A fraction of the kinetic energy and momentum, ϵ_r and μ_r, respectively, is kept by the impacting grain leading to its rebound. The remaining fraction is only partly transferred to the ejected grains, as a fraction of the impacting energy and momentum, ϵ_f and μ_f, respectively, leads to the rearrangement of surface grains and, consequently, to friction related losses.

Both the energy and momentum conservation equations are solved for N by statistically representing the kinetic energy and momentum of the ejected grains by their mean values. Only the horizontal direction of the momentum equation is taken into account as the vertical component of the impact velocity is relatively small (Bagnold, 1941). Comola and Lehning (2017) arrived at the following expressions:

$$N_E = \frac{(1 - P_r\epsilon_r - \epsilon_f)\, m_I u_{p,I}^2}{\langle m\rangle\langle u_{p,o}^2\rangle + r_E\sigma_m\sigma_{u_{p,o}^2} + 2\phi} \tag{8a}$$

$$N_M = \frac{(1 - P_r\mu_r - \mu_f)\, m_I u_{p,I}\cos\alpha_I}{\langle m\rangle\langle u_{p,o}\rangle\langle\cos\alpha\rangle\langle\cos\beta\rangle + r_M\sigma_m\sigma_{u_{p,o}}} \tag{8b}$$

where N_E and N_M denote the number of ejected grains computed by the energy and momentum equations, respectively. The quantities within angle brackets represent average values, m being the mass of an ejected grain, α the vertical angle of ejection and β the horizontal angle of ejection measured from the plane of impact (in the above equations, both α and β are assumed statistically independent). σ_m, $\sigma_{u_{p,o}}$ and $\sigma_{u_{p,o}^2}$ denote the standard deviation of m, $u_{p,o}$ and $u_{p,o}^2$, respectively. α_I is the vertical angle of impact, r_E and r_M are the correlation coefficients between m and $u_{p,o}^2$ and between m and $u_{p,o}$, respectively, and ϕ is the energy required to break the cohesive bonds between each ejected grain and the surrounding ones. The modulus symbol in both $u_{p,o}$ and $u_{p,I}$ was suppressed for simplicity.

The number of ejected grains is then given by the minimum value between N_E and N_M, which guarantees that neither energy nor momentum is created. The number of ejected grains is expected to be restricted by momentum conservation when the bed is constituted by loose grains (Kok & Renno, 2009). However, this is not always obtained when interparticle forces are present (Shao et al., 1993; Comola & Lehning, 2017).

The ejection velocity is assumed to follow an exponential distribution (Anderson & Haff, 1988, 1991). The values considered for the mean ejection velocity and the vertical and horizontal angles of ejection are presented in Table 1. The mean and standard deviation of the mass of ejected grains are computed assuming equally-sized grains or a lognormal distribution for the grain diameter (Colbeck, 1986).

Table 2. Parameters of the splash model.

Parameter	Values used in the model	References
ϵ_r	0.25	Rice et al. (1995); D. Wang et al. (2008)
ϵ_f	$0.96\,(1 - P_r\epsilon_r)$	Ammi et al. (2009)
μ_r	$\sqrt{\epsilon_r}$	-
μ_f	0.4	Rice et al. (1995)
r_E	0	-
r_M	0	-
$\langle\cos\alpha\rangle$	0.75	Rice et al. (1995)
$\langle\cos\beta\rangle$	0.96	Xing and He (2013)
$\phi^{(1)}$ [J]	$10^{-10}, 5{\times}10^{-10}, 5{\times}10^{-9}$	Gauer (2001)

$^{(1)}$ Values obtained for ice particles. $\phi = 0$ J is considered for loose grains.

The parameters $\epsilon_r, \epsilon_f, \mu_r, \mu_f, r_E, r_M, \langle \cos\alpha \rangle$ and $\langle \cos\beta \rangle$ are assumed constant. ϕ is set to different figures throughout the simulations. The values used in the model are presented in Table 2. They are defined according to the range proposed in the literature (Comola & Lehning, 2017). The correlation coefficients, r_E and r_M, are set to zero in this work, as estimates of these parameters developed for snow beds are not available in the literature.

3 Numerical setup

3.1 General settings

The computational domain is a cube of 6.4 m side length. It models the near surface atmospheric flow over a flat erodible bed. The domain is relatively short in both horizontal directions, specially in the streamwise one. This is partially compensated by applying periodic boundary conditions. However, the use of a longer domain is necessary for the consistent development of large coherent structures observed in experimental and numerical boundary layer studies (Munters et al., 2016). Even though longer domains are imperative for a proper comparison with experimental data, a cubic domain was considered adequate for the study of steady state saltation developed in this paper. Moreover, it greatly reduces the computational time.

The domain is discretized in 64 cells of equal size in the streamwise and crosswise directions. The vertical direction is discretized in 128 cells using a hyperbolic function, which guarantees a more refined mesh close to the bottom boundary. The first grid node above the surface is placed in the logarithmic sublayer.

The simulations are performed over a total of 350 s to allow the development of steady state saltation. The time step is set to $5{\times}10^{-5}$ s. The flow is allowed to develop over 25 s prior to the start of surface erosion.

The initial streamwise component of the velocity field is given by a logarithmic profile, function of u_* and of the roughness length, z_o. The roughness length is assumed constant along the surface and equal to 10^{-5} m. The initial crosswise and vertical velocity components are set to zero. Noise is added to all velocity components.

The fluid density and kinematic viscosity are set to $\rho_f = 1.34$ kg m^{-3} and $\nu_f = 1.24{\times}10^{-5}$ m^2 s^{-1}, respectively. Particles are modelled as ice spheres with density $\rho_p = 918.4$ kg m^{-3}. The top of the erodible surface is defined at a height $z = 0$ m and particle size is assumed uniform or defined by a lognormal distribution, characterized by the grain mean diameter, $\langle d \rangle$, and standard deviation, σ_d. In order to reduce the computational cost of the simulations, particles are not modelled individually but grouped in parcels, constituted by particles of equal size that follow the same trajectory.

3.2 Simulation details

In order to study the effect of friction velocity, mean grain size, size distribution and cohesion energy on saltation dynamics, four groups of simulations are performed - S1 to S4 - for which different values of u_*, $\langle d \rangle$, σ_d and ϕ are considered. The parameters used in each simulation group are summarized in Table 3.

In simulations S1 and S2, a bed of equally-sized ($\sigma_d = 0$ μm) and loose grains ($\phi = 0$ J) is modeled. In S1, the effect of the imposed friction velocity is studied while keeping the remaining parameters unchanged. In S2, different values for the grain diameter, $\langle d \rangle$, are tested. In simulations S3 and S4, a bed of mixed-sized grains is modeled by describing the grain size by a lognormal distribution. In S3, the effect of the standard deviation of the distribution, σ_d, on steady state saltation is analyzed. Finally, in S4, interparticle forces are assumed between surface grains and different values for the cohe-

Table 3. Simulation input parameters.

	Description	u_* [m s^{-1}]	$\langle d \rangle$ [μm]	σ_d [μm]	ϕ [J]
S1	Effect of friction velocity	0.3 - 0.8	200	0	0
S2	Effect of mean grain diameter	0.4 - 0.8	100, 300, 400	0	0
S3	Effect of size distribution	0.4 - 0.8	200	100, 200	0
S4	Effect of cohesion	0.4 - 0.8	200	100	$10^{-10}, 5{\times}10^{-10}, 5{\times}10^{-9}$

sion energy, ϕ, are tested. Different values for u_* are also considered in simulations S2 to S4. The fluid threshold coefficient is set to $A = 0.1$ and the splash model parameters are set to the values presented in Table 2.

3.3 Data post-processing

The vertical profiles of particle concentration, mean particle streamwise velocity and particle mass flux are computed by dividing the computational domain in horizontal layers of thickness Δz_k.

The particle concentration, c [kg m^{-3}], is given by

$$c(z_k) = \frac{\sum_{n=1}^{N_k} m_n}{L_x L_y \Delta z_k} \tag{9}$$

where N_k is the number of particles in the horizontal layer with mean height z_k, m_n is the mass of the n^{th} particle, L_x is the domain length and L_y is the domain width.

The mean particle velocity in the streamwise direction, $\langle u_{p,1} \rangle$, is given by the mass-weighted average:

$$\langle u_{p,1} \rangle (z_k) = \frac{\sum_{n=1}^{N_k} m_n u_{p,1_n}}{\sum_{n=1}^{N_k} m_n} \tag{10}$$

where $u_{p,1_n}$ is the streamwise velocity of the n^{th} particle in layer k.

The particle mass flux, q [kg m^{-2} s^{-1}], is given by the product of particle concentration and mean particle streamwise velocity, yielding

$$q(z_k) = \frac{\sum_{n=1}^{N_k} m_n u_{p,1_n}}{L_x L_y \Delta z_k}. \tag{11}$$

The integrated mass flux of saltating particles, Q [kg m^{-1} s^{-1}], is computed by integrating particle mass flux, q, along the height, from the surface to 0.15 m. The last 100 s of each simulation are used to compute the time-averaged values of c, $\langle u_{p,1} \rangle$, q and Q. During this time interval (250 s - 350 s), the changes in total mass of particles aloft are negligible and saltation is assumed to be in steady state.

The surface friction velocity, $u_{*,s}$, at each time step is obtained by averaging over the surface. The time-averaged value obtained for the last 100 s of each simulation is defined as the equilibrium surface friction velocity, $u_{*,eq}$.

4 Results and discussion

In this section, the results are presented and discussed. Results obtained with simulations S1 to S4 are analyzed in sections 4.1 to 4.4, respectively. Moreover, a comparison with existing saltation models and with the conclusions drawn from the latest wind tunnel and field experiments is presented.

4.1 The effect of friction velocity

In simulations S1, a bed of equally-sized and loose grains with a diameter of 200 μm is modelled. The streamwise wind speed profiles are presented in Figure 1. They are computed by averaging the streamwise velocity along horizontal planes. The profiles are time-averaged over the first 25 s and over the last 100 s of each simulation (before saltation onset and during steady state saltation). As expected, the resulting wind speed is lower for the latter, as the saltation layer acts on the flow as an additional sink of momentum.

A focus point can be observed at approximately 7 mm above the surface for the velocity profiles obtained during steady state saltation (inset in Figure 1). This focus point was originally observed by Bagnold (1941) and is given by the interception of velocity profiles obtained during saltation with different friction velocities. It was used as a simplifying assumption in previous saltation models (Pomeroy & Gray, 1990) and reproduced by several numerical models based on parameterizations of splash entrainment (Kok et al., 2012).

An equivalent surface roughness, characteristic of each saltation layer, can be estimated from the velocity profiles obtained during steady state saltation (Dupont et al., 2013). By extending the velocity profiles down to the wall, zero velocity is attained at greater heights as u_* increases. Hence, the equivalent surface roughness increases with u_*. This is related to an enhanced momentum exchange between the fluid flow and the particles aloft when u_* increases. Therefore, it is ultimately related to the increase in particle mass flux.

The time-averaged vertical profiles of particle mass flux, concentration and mean streamwise velocity are presented in Figures 2a-c. The average is performed over the last 100 s of each simulation. Particle mass flux decreases with height and increases with u_*

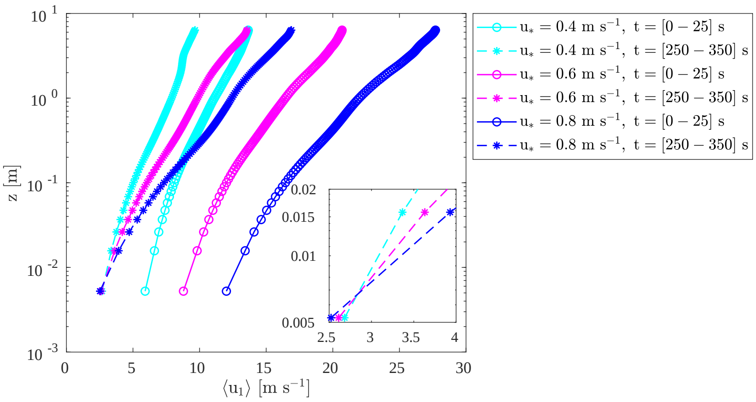

Figure 1. Vertical profiles of mean streamwise wind speed obtained before saltation onset and during steady state saltation (simulations S1). The inset is a zoom-in to the near surface region during saltation.

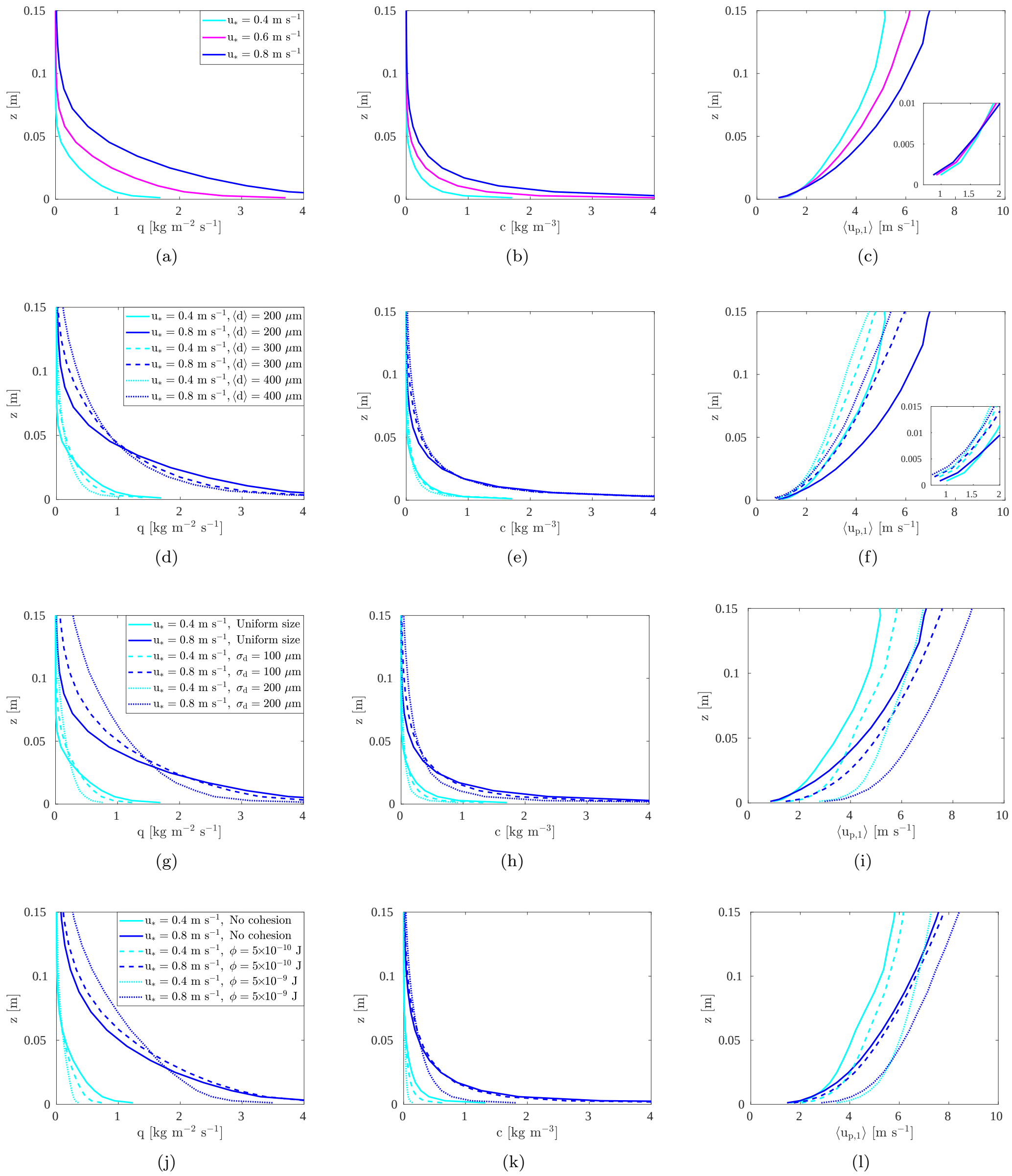

Figure 2. Vertical profiles of particle mass flux, concentration and streamwise velocity obtained with simulations S1 (a-c), S2 (d-f), S3 (g-i) and S4 (j-l). In (d-i) and (j-l) results from simulations S1 and S3 are presented for comparison, respectively. All values are obtained from surface averages and time averages over the last 100 s of each simulation. The insets in (c) and (f) are a zoom-in to the near surface region.

(Figure 2a), as previously observed in field measurements (Nishimura et al., 2014). A similar trend is observed for particle concentration (Figure 2b). As expected, particle streamwise velocity increases with height and u_* (and, therefore, with wind speed), as shown in Figure 2c. For heights smaller than 1 cm (approximately), the variation of particle streamwise velocity with u_* is negligible (inset in Figure 2c). This is predicted by existing saltation models (Kok & Renno, 2009) and wind tunnel measurements (Ho et al., 2011). This result is also obtained theoretically, based on the notion that steady state saltation is characterized by a mean replacement capacity equal to one (Kok et al., 2012). This means that, on average, one grain enters the saltation layer each time an impacting grain fails to rebound. Assuming that saltation is mainly dominated by splash, this condition is met for a given impact velocity, which completely defines the number of ejected grains and the probability of rebound for a given bed type (see equations 7 and 8). Hence, it follows that the particle speed near the surface is independent of u_* and rather varies with the bed characteristics. The near surface particle speed is closely linked to the focus point (or Bagnold's focus) observed in the average streamwise wind speed profiles (Figure 1). Saltating particles are accelerated by the flow along their trajectories, therefore, the near surface particle speed can only be approximately invariant with regards to u_* if the near surface wind speed is also approximately invariant with regards to the same quantity. High above the surface, the wind speed increases as u_* rises. Hence, a near surface wind speed approximately invariant with u_* is only obtained if a focus point is visible close to the surface, below which the wind speed decreases as u_* increases.

The surface friction velocity, $u_{*,s}$, as a function of time is presented in Figure 3. The fluid threshold friction velocity is also plotted as a reference. $u_{*,s}$ strongly decreases immediately after the start of surface erosion ($t = 25$ s). It tends to an equilibrium value - the equilibrium surface friction velocity, $u_{*,eq}$. A small reduction of $u_{*,eq}$ is obtained when the imposed friction velocity, u_*, increases (inset in Figure 3). The numerical model COMSALT proposed by Kok and Renno (2009) also predicts this trend for a bed with uniform grain size (Kok et al., 2012). However, they predicted a stronger reduction than that presented in the inset in Figure 3. The wind tunnel experiments performed by Walter et al. (2014) revealed a non-monotonic evolution of $u_{*,eq}$ with u_*. During the experiments, u_* was continuously increased above the fluid threshold. As a result, the measured $u_{*,eq}$ firstly reduced and then increased. In general, a relatively small variation of $u_{*,eq}$ with u_* and a relatively large standard deviation of the measurements were obtained, which may be partially related to changes in the snow cover during the experiments. Based on

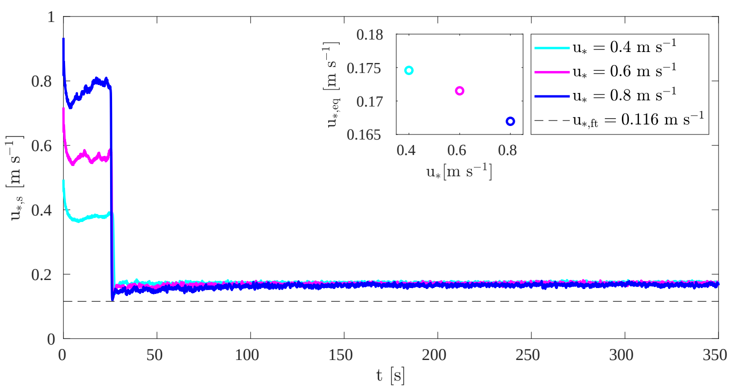

Figure 3. Surface friction velocity obtained with simulations S1. The fluid threshold friction velocity is also presented as a reference. In these simulations, saltation is allowed to develop after the first 25 seconds. The equilibrium friction velocity is presented in the inset.

these results, Walter et al. (2014) considered the assumption of a constant surface friction velocity (function of the grain type but invariant with the wind speed, as proposed by Owen (1964)) a reasonable first-order approximation.

The impact threshold, $u_{*,it}$, is generally defined as the minimum friction velocity, u_*, at which saltation can be sustained after its onset (Bagnold, 1941). In the work of Kok and Renno (2009), the impact threshold is assumed equal to the minimum value of u_* that satisfies the steady state equation. In their model, the equilibrium friction velocity, $u_{*,eq}$, tends to the computed impact threshold as u_* decreases (Kok et al., 2012). Taking into account these results, a simplified approach is followed in this work and $u_{*,it}$ is given by the value of $u_{*,eq}$ obtained when u_* is set to 0.4 m s^{-1} (the minimum friction velocity common to all simulation groups). This approach is considered appropriate taking into account the small variation of $u_{*,eq}$ with u_* obtained for most simulations. A more accurate estimation of the impact threshold needs further investigation, in particular, a set of simulations at low friction velocities (near the impact and fluid thresholds) and the analysis of the transition from intermittent to steady state saltation.

The mass of particles aloft per unit surface area varies with time, as presented in Figure 4. The vertical mass flux of particles leaving the surface either through aerodynamic entrainment or splash and the vertical mass flux of particles deposited due to failure of rebound are also presented. The results were obtained for $u_* = 0.4$ m s^{-1}. The evolution shown is representative of all the simulations performed. At $t = 25$ s, saltation starts due to aerodynamic entrainment. A sudden increase in the mass of particles aloft is observed, which is consistent with the strong decrease in surface friction velocity presented in Figure 3. The overshoot in particle mass is justified by the surge in the vertical mass flux of particles entering saltation via splash, that overcomes the vertical mass flux of particles leaving the saltation layer through deposition (Figure 4b). The imbalance between the vertical mass flux of splash and deposition drives the variation of mass of particles aloft. When saltation reaches steady state, a dynamic equilibrium between the vertical mass flux of splash and deposition is obtained. Aerodynamic entrainment is much smaller than splash: the vertical mass flux reaches a maximum at saltation onset and then decreases to a steady state value, which is one order of magnitude lower than the vertical mass flux of splash and deposition. In the simulations performed, aerodynamic entrainment occurs during steady state saltation because the surface friction velocity is greater than the specified fluid threshold (Figure 3). However, taking into

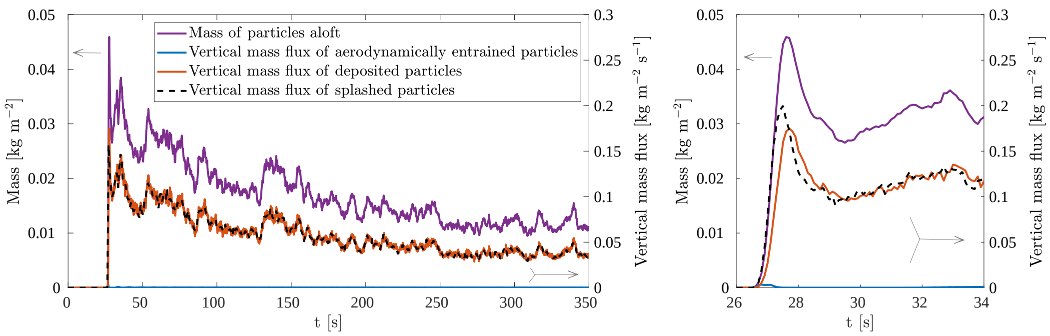

(a) Complete time-evolution

(b) First seconds after saltation onset

Figure 4. Time-evolution of the mass of particles aloft per unit area (purple line). The time-evolution of the vertical mass flux of particles leaving the surface either through aerodynamic entrainment or splash and the vertical mass flux of particles deposited are presented in blue, dashed black and orange, respectively. Results obtained from simulation S1 with $u_* = 0.4$ m s^{-1}. The arrows indicate the y-axis corresponding to each curve.

account the relatively small contribution of aerodynamic entrainment to the mass of particles aloft, the correct assessment of the fluid threshold is expected to have a negligible effect on steady state saltation for friction velocities significantly greater than the fluid threshold. These results are in agreement with the well-established notion that steady state saltation is dominated by splash and that an equilibrium between splash and failure of rebound should be attained (Kok et al., 2012).

The time-averaged integrated mass flux and the corresponding standard deviation are presented in Figure 5. In Figure 5a, the fit between the mean values and a quadratic function is presented, as well as between the mean values and a cubic function. In Figure 5b, the results are compared to saltation models proposed by several authors (Bagnold, 1941; Pomeroy & Gray, 1990; Doorschot & Lehning, 2002; Sørensen, 2004; Durán et al., 2011). The results from Doorschot and Lehning (2002) were obtained from the numerical algorithm proposed by the authors. The remaining curves are computed from the equations presented in Table 4.

Equations used to compute the integrated mass flux (as those presented in Table 4) are obtained from the balance of horizontal momentum applied to the saltating particles. The total horizontal force per unit area applied on these particles is equal to the excess shear stress, $\tau - \tau_s = \rho_f \left(u_*^2 - u_{*,s}^2\right)$, where $\tau = \rho_f u_*^2$ is the surface shear stress before saltation onset. In addition, if particle trajectories are characterized by a representative hop, with length L, in which particles undergo a mean variation of horizontal velocity, Δu_{p_h}, between lift off and impact with the bed, the integrated mass flux is computed from $Q = \rho_f \left(u_*^2 - u_{*,s}^2\right) L/\Delta u_{p_h}$ (e.g., Kok et al., 2012). Different models arise from different assumptions regarding the evolution of $u_{*,s}$ and $L/\Delta u_{p_h}$. Following Owen's hypothesis (Owen, 1964), the surface friction velocity, $u_{*,s}$, is generally assumed invariant with respect to u_* and equal to the impact threshold, $u_{*,it}$. Even though there is no full consensus on the validity of this hypothesis and its implications on saltation dynamics (see, for instance, Kok et al. (2012) and Walter et al. (2014)), the fact that the general equation yields $Q = 0$ when u_* equals $u_{*,s}$ favours the use of this simplifying assumption. The quadratic growth of Q with u_* is predicted theoretically when both the particle velocity near the surface (and, consequently, Δu_{p_h}) and the representative hop length are considered invariant with u_* (Ungar & Haff, 1987; Durán et al., 2011). This yields an expression for Q of the form au_*^2+b, which is corroborated by recent field experiments (e.g., Martin & Kok, 2017). The increase of Q with u_*^3 was early proposed by

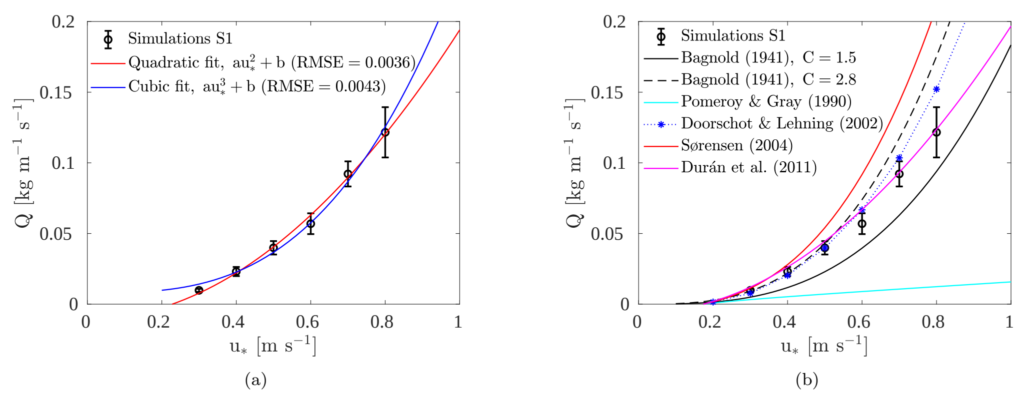

Figure 5. Integrated mass flux obtained with simulations S1. The error bar is twice the standard deviation of the results. (a) Fit of simulation results to quadratic and cubic functions (RMSE is the root mean square error of the fit). (b) Comparison with saltation models.

Table 4. Saltation models for the integrated mass flux, Q.

Integrated mass flux	Constant parameters	References
$Q_{Bag} = C\sqrt{\frac{\langle d\rangle}{d_R}}\frac{\rho_f}{g}u_*^3$	$C = 1.5$ (uniform grains) $C = 2.8$ (highly non-uniform grains)	Bagnold (1941)
$Q_{P\&G} = C\frac{\rho_f}{g}u_{*,it}u_*\left(1-\frac{u_{*,it}^2}{u_*^2}\right)$	$C = 0.68$	Pomeroy and Gray (1990)
$Q_{S\o} = \frac{\rho_f}{g}u_*^3\left(1-\frac{u_{*,it}^2}{u_*^2}\right)\left(\alpha+\beta\frac{u_{*,it}^2}{u_*^2}+\gamma\frac{u_{*,it}}{u_*}\right)$	$\alpha = 2.6$, $\beta = 2.5$, $\gamma = 2.0$ (1)	Sørensen (2004)
$Q_{Dur} = C\frac{\rho_f}{g}u_{*,it}u_*^2\left(1-\frac{u_{*,it}^2}{u_*^2}\right)$	$C = 8.5$ (2)	Durán et al. (2011)

d_R is a reference diameter, $d_R = 250$ μm.

(1) Constant parameters proposed by Vionnet et al. (2014) to model snow saltation.

(2) C estimated from Figure 27 in Durán et al. (2011), assuming a packing fraction of the bed, ϕ_b, equal to 0.95.

Bagnold (1941) based on the assumptions that L is proportional to u_*^2 and that the near surface particle velocity increases linearly with u_*. This yields an expression for Q of the form au_*^3+b. A cubic expression for the integrated mass flux can also be obtained by assuming that particle velocity near the surface is invariant with u_*, but considering a linear increase of L with u_* (Sørensen, 1991, 2004). However, experiments show that a cubic increase of Q with u_* is only likely to happen when saltation develops over rigid beds (Ho et al., 2011).

In Figure 5a, a good agreement is obtained for both polynomial functions, although the quadratic fit is slightly better (root mean square error, RMSE, equal to 0.0036 instead of 0.0043). In fact, for the range of studied friction velocities, small differences between the two functions are obtained.

In Figure 5b, the comparison between simulation results and saltation models is made by assuming an impact threshold of 0.175 m s^{-1} (the value of $u_{*,eq}$ obtained for $u_* = 0.4$ m s^{-1}, as previously discussed). In the models proposed by Pomeroy and Gray (1990), Sørensen (2004) and Durán et al. (2011), the impact threshold is a parameter in the integrated mass flux equations which characterizes the erodible bed (Table 4). For friction velocities lower than 0.6 m s^{-1}, a good agreement is seen between simulation results and the saltation model proposed by Doorschot and Lehning (2002). At higher friction velocities, the model proposed by Doorschot and Lehning (2002) predicts greater values for Q and a better agreement is obtained with the expression proposed by Durán et al. (2011). Q_{Dur} scales with u_*^2, which is supported by the current simulation results. However, this equation is highly sensitive to the value of the impact threshold and the observed agreement is greatly compromised for different values of $u_{*,it}$. Bagnold (1941) and Sørensen (2004) proposed expressions for Q proportional to u_*^3. When using the coefficients proposed by Vionnet et al. (2014), a greater mass flux is obtained with Sørensen's expression in comparison with the simulation results. Conversely, the expression proposed by Bagnold (1941) to describe saltation over uniform grains ($C = 1.5$) predicts lower values for Q. For friction velocities lower than 0.6 m s^{-1}, the simulation results agree well with the model proposed by Bagnold (1941) if the constant parameter C is increased to 2.8. However, the curve obtained with $C = 2.8$ is only expected to describe saltation over a bed of mixed-sized grains. The expression proposed by Pomeroy and Gray (1990) underestimates the integrated mass flux in comparison with the remaining models and the simulation results. This is partly justified by the authors assumption of a relatively shallow saltation layer (saltation layer height varying from 7 mm to 5 cm for u_*

varying from 0.3 to 0.8 m s^{-1}). However, even by adjusting the height of integration from 15 cm to the proposed values, the integrated mass flux obtained with the current numerical model is significantly greater that the evolution proposed by Pomeroy and Gray (1990). Hence, the deviation between $Q_{P\&G}$ and the remaining models and simulation results is mainly related to the erroneous scaling of the integrated mass flux with u_*.

4.2 The effect of mean grain diameter

In this section, we continue the analysis of saltation over a bed of equally-sized grains. The effect of grain size is studied by comparing the results presented in the previous section (S1, $\langle d \rangle = 200$ μm) with those from simulations S2, obtained for different grain sizes.

The vertical profiles of particle mass flux, concentration and mean streamwise velocity obtained for grain diameters ranging from 200 to 400 μm are presented in Figures 2d-f. It can be observed that particle streamwise velocity decreases when the grain size increases (Figure 2f). This is due to the fact that aerodynamic drag applied to the saltating particles increases approximately with d^2, but particle mass increases with d^3. Hence, the ability of the flow to accelerate the saltating grains reduces with particle mass. The near surface particle velocity also decreases with the grain diameter (inset in Figure 2f). Although the near surface particle velocity does not vary significantly with u_*, it clearly varies with the grain size.

As the grain size increases, the particle mass flux decreases near the surface and increases at higher elevations of the saltation layer (Figure 2d). Near the surface, this trend is justified by the decrease in particle streamwise velocity as $\langle d \rangle$ increases (Figure 2f). Above approximately 4 cm, the increase in particle mass flux as the grain size increases is due to the rise in particle concentration (Figure 2e), which is related to both an increase in particle mass and the number of particles aloft. The vertical profiles of particle mass flux obtained for $u_* = 0.4$ m s^{-1} are also presented in logarithmic scale in Figure 6a. The results obtained with $\langle d \rangle = 100$ μm are added for comparison. An exponential decay along the saltation layer is clear for the greater grain sizes ($\langle d \rangle$ between 200 and 400 μm), which is in agreement with field measurements (Martin & Kok, 2017). The vertical profile obtained with the smallest grain size ($\langle d \rangle = 100$ μm) differs significantly from the others. A similar trend inside the saltation layer is visible up to 1 cm height. However, at greater heights, the profile assumes a different shape suggesting transition from saltation to suspension. In fact, for the smallest grain size, particles can be

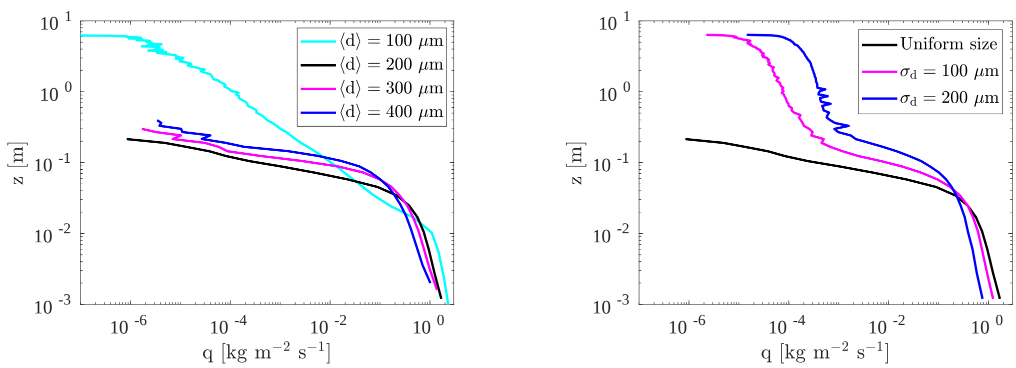

(a) (b)

Figure 6. Vertical profiles of particle mass flux obtained with simulations S2 (a) and S3 (b) for $u_* = 0.4$ m s^{-1}. Results from simulations S1 are presented for comparison.

observed up to the top of the domain, while for greater grain sizes, aeolian transport seems to occur via saltation only as the mass flux profiles follow an exponential decay up to the maximum height reached by the particles (14 cm, approximately).

The integrated mass flux is presented in Figure 7a along with the expression proposed by Bagnold (1941) and the numerical results from Doorschot and Lehning (2002) for varying mean grain diameters and friction velocities. Bagnold's expression establishes that Q is proportional to $\langle d \rangle^{\frac{1}{2}}$. The numerical model of Doorschot and Lehning (2002) also predicts an increase in the integrated mass flux with the grain diameter. In contrast, a negligible variation is obtained with our model for grain diameters ranging from 200 to 400 μm: the reduction in mass flux near the surface and its increase at higher elevations for increasingly bigger grains (Figure 2d) counterbalance each other. In fact, other saltation models do not predict an explicit variation of Q with particle mean diameter (e.g., Sørensen, 2004; Durán et al., 2011). The wind tunnel measurements carried out by Dong et al. (2003) revealed a reduction in the integrated mass flux with the grain diameter. However, the comparison between sand beds is performed considering the same wind speed at a given reference height. Hence, it is observed that for the same wind speed at the chosen reference height, the integrated mass flux decreases as the grain size increases. In the simulations performed, the imposed friction velocity is kept constant when varying the grain size, which implies different velocities at a given reference height, depending on the mass flux of saltating particles and the respective momentum transfer. The negligible variation of the integrated mass flux with $\langle d \rangle$ obtained with our model goes along with an increase in the wind speed at all heights as the grain size increases. When analyzing the experiments of Dong et al. (2003) performed with different grain sizes but yielding similar integrated mass fluxes, a greater wind speed is also obtained for greater grain sizes.

When considering a uniform bed with grains of 100 μm, a greater integrated mass flux is obtained. However, as previously discussed, particles between 1 and 15 cm height might not be in saltation but rather in suspension. When modeling particles smaller than

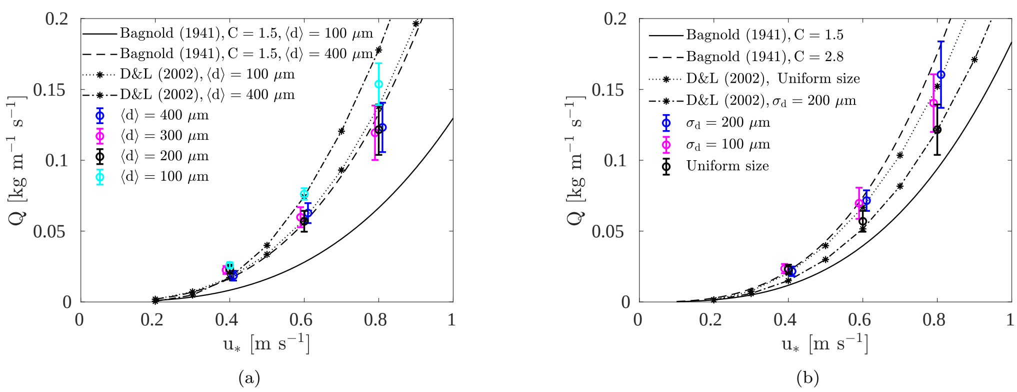

Figure 7. Integrated mass flux obtained with simulations S2 (a) and S3 (b) for u_* equal to 0.4, 0.6 and 0.8 m s^{-1}. Results from simulations S1 obtained with the same u_* are also presented for comparison. To improve readability, some data points are slightly shifted in the u_* axis. The error bar is twice the standard deviation of the results. The curves are obtained from Bagnold's model (Q_{Bag} in Table 4) and from the numerical model proposed by Doorschot and Lehning (2002) (D&L). In (a), the curves are computed considering a uniform bed characterized by different grain diameters. In (b), both a uniform and a mixed-sized bed with a mean grain diameter of 200 μm are considered.

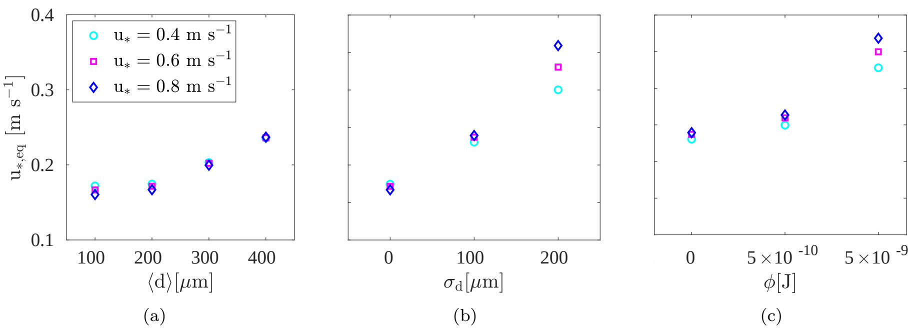

Figure 8. Equilibrium friction velocity obtained with simulations S2 (a), S3 (b) and S4 (c). In (a) and (b), results from simulations S1 are presented for comparison. In (c), results from simulations S3 are presented for comparison.

200 μm, a rigorous definition of the saltation layer height is needed to fully assess the impact of the mean diameter on the integrated mass flux in saltation.

The equilibrium surface friction velocity varies considerably with the mean grain size. In Figure 8a, an increase of $u_{*,eq}$ is observed when $\langle d \rangle$ increases for values greater than 200 μm, which is consistent with the results of Kok and Renno (2009). For a given u_*, the total momentum transfer from the fluid to the particles decreases for greater grain diameters. This is partly due to a smaller number of particles aloft, which overcomes the increase in drag applied on each grain.

4.3 The effect of mixed-sized grains

In order to model saltation over a bed of mixed-sized grains, the size distribution of surface grains is described by a lognormal distribution. In this section, the results from simulations S3, obtained with different standard deviations of the grain diameter, are presented and compared with those from simulations S1, obtained with a uniform grain size.

The vertical profiles of particle mass flux, concentration and mean streamwise velocity are presented in Figures 2g-i. Grain size heterogeneity leads to a greater mean particle streamwise velocity, both near the surface and at higher elevations (Figure 2i). This is due to an increase in the number of smaller particles aloft, which are easily accelerated by the fluid flow. Similarly to Figure 2f (simulations S2), the variation of particle speed close to the surface with u_* is negligible; however, a clear variation with the bed characteristics is observed.

Figures 2g and 2h show that grain size heterogeneity decreases particle mass flux and concentration close to the surface but leads to greater values at higher elevations of the saltation layer. The vertical profiles of particle mass flux obtained for $u_* = 0.4$ m s^{-1} are presented in logarithmic scale in Figure 6b. As expected, close to the surface, an exponential decay across the saltation layer is observed. At higher elevations, a cloud of suspended grains forms above the saltation layer of mixed-sized beds and a second distinct exponential decay of the mass flux along the height is observed. The transition from saltation to suspension occurs at approximately 12 cm and is characterized by the change in gradient of the mass flux profiles. This trend was previously observed in field measurements (Gordon et al., 2009) and other numerical models (e.g., Nemoto & Nishimura, 2004).

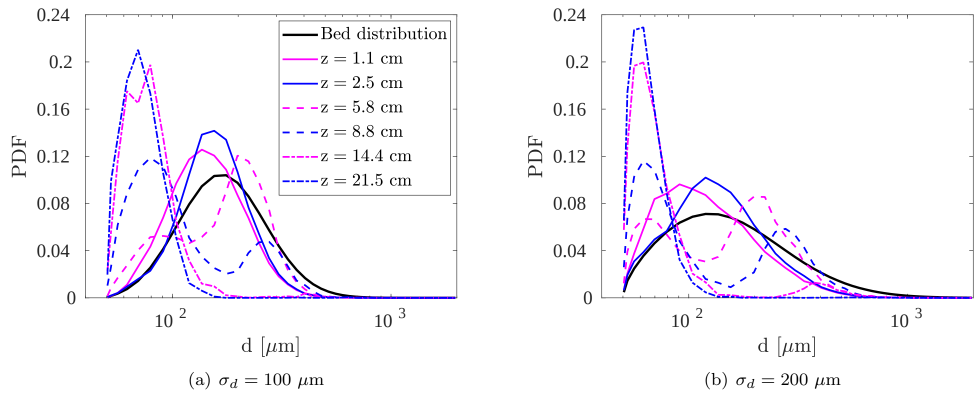

Figure 9. Probability density function (PDF) of particle size at the bed and at different heights obtained from simulations S3 considering $u_* = 0.4$ m s^{-1}.

The probability density function (PDF) of particle size at different heights is presented in Figure 9 for $u_* = 0.4$ m s^{-1} and both size distributions (σ_d of 100 and 200 μm). The PDF of particle size at the bed is also presented for comparison (the left tail of the distribution is not obtained, as a minimum grain size of 50 μm is specified in the simulations). Below approximately 3 cm height, the size distribution of particles aloft is reasonably well approximated by a lognormal distribution. It is similar to the PDF at the bed, but skewed towards smaller grain sizes. From 5 to 10 cm height, a bi-lognormal distribution is visible in both simulations. In this region, for progressively greater heights, the probability density of smaller grains increases and the probability density of bigger grains decreases. Finally, above approximately 14 cm, a new lognormal distribution arises, characterized by grains smaller than 100 μm. The presented variation of particle size distribution with height agrees well with the results of Nemoto and Nishimura (2004) and is related to the saltation-suspension transition observed in Figure 6b.

Figure 9b shows that a wider lognormal bed size distribution leads to smaller grain sizes in the first centimeters above the surface. Smaller grains and less particles aloft justify the decrease in mass flux close to the surface observed in Figure 6b. Moreover, the fraction of grains within the range 200 to 500 μm present between 8 and 15 cm height is greater. Considering that these particles are transported in saltation, this is in agreement with the increase in saltation layer height observed in Figure 6b.

The integrated mass flux is presented in Figure 7b. The simulation results are compared with Bagnold's model, considering different values for the parameter C (Bagnold, 1941), and with the results of the numerical model proposed by Doorschot and Lehning (2002). In the latter, particle size is assumed uniform ($\langle d \rangle = 200$ μm) or defined by a lognormal distribution ($\langle d \rangle = 200$ μm, $\sigma_d = 200$ μm). In general, the integrated mass flux obtained with the current model increases with bed heterogeneity. This trend is also predicted by Bagnold (1941). However, it contrasts with the evolution obtained with the model of Doorschot and Lehning (2002), in which Q decreases when the bed heterogeneity increases. The effect of bed size distribution on the integrated mass flux underlines the importance of correctly describing particle size when estimating snow saltation mass flux. According to the simulation results, this is particularly relevant when u_* is greater than 0.4 m s^{-1}. Even though a rigorous definition of the saltation layer height is not taken in this work, similar trends are obtained when the integration height is limited to the first 10 cm. Moreover, the effect of bed heterogeneity on the computed integrated mass flux is even more significant if the suspension layer is taken into account. The integrated mass flux obtained for a uniform bed of grains with 100 μm in diameter is closer to the values obtained for the studied mixed-sized beds, compared to the other uniform beds with larger grains (Figure 7a). However, over the uniform bed with grains of 100 μm, particles above 1 cm height seem to be transported in suspension (Figure 6a). Taking also into account that an increase in the mean particle diameter from 200 to 400 μm leads to a negligible variation of Q (Figure 7a), it is in general not possible to correctly model saltation over a mixed-size bed considering a representative diameter and equally-sized grains.

An increase in bed heterogeneity also leads to an increase in the equilibrium surface friction velocity, $u_{*,eq}$ (Figure 8b). In contrast with the simulations performed over equally-sized grains, $u_{*,eq}$ slightly increases with u_*. This trend is specially visible for the results obtained with $\sigma_d = 200$ μm. For a given u_*, the total exchange of momentum from the fluid to the particles decreases for greater standard deviations of the size distribution. Taking into account that the drag applied on each grain is approximately proportional to d^2 and that the number of particles aloft does not vary in a monotonous way with σ_d, the decrease in the momentum exchange is explained by the presence of particles with diameters smaller than the mean value ($\langle d \rangle = 200$ μm).

4.4 The effect of interparticle cohesion

We complete the analysis of mixed-sized bed saltation by studying the effect of interparticle cohesion. In this section, the results obtained with simulations S4 are presented. A bed of mixed-sized grains characterized by a lognormal distribution with $\langle d \rangle =$ 200 μm and $\sigma_d = 100$ μm is considered. The results are compared with those from simulation S3, that were performed with the same particle size distribution but neglecting interparticle cohesion.

The vertical profiles of particle mass flux, concentration and mean streamwise velocity are presented in Figures 2j-l. As cohesion energy increases, the mass flux and particle concentration decrease close to the surface and increase at higher regions of the saltation layer (Figures 2j,k). Particle mean streamwise velocity increases with cohesion energy at all heights (Figure 2l). As expected, close to the surface, a negligible variation of particle streamwise velocity is obtained for different u_*; however, a clear variation with interparticle cohesion is seen. Hence, the decrease in mass flux near the surface is due to a strong reduction in the number of particles there and its increase at higher elevations is justified by the rise of both the number of particles aloft and the particle streamwise velocity.

The equilibrium friction velocity, $u_{*,eq}$, is presented in Figure 8c. It is expected to vary with the bed type, and therefore, with the strength of the interparticle bonds. In fact, $u_{*,eq}$ increases with the cohesion energy, which was also obtained by Comola, Gaume, et al. (2019).

Cohesion energy has a direct effect on the number of ejected grains computed from energy conservation, N_E (see equation 8a). If N_E becomes smaller than N_M, the number of ejected grains is restricted by energy conservation and it decreases for increasing values of ϕ. Hence, for the same impact velocity and impacting grain diameter, the number of splashed grains reduces with cohesion energy (Comola & Lehning, 2017). Our results suggest that this leads to a global decrease in the number of particles aloft. As a result, for greater values of cohesion energy, the total momentum transfer from the fluid to the particles is smaller (Figure 8c), as well as the consequent decrease in streamwise wind speed. This leads to a general increase in particle speed. The initial velocity at which the splashed grains are ejected from the bed does not vary directly with interparticle cohesion (see distribution characteristics presented in Table 1). However, greater impact velocities lead to higher ejection velocities.

The integrated mass flux is presented in Figure 10. The results obtained with the saltation models proposed by Pomeroy and Gray (1990), Doorschot and Lehning (2002) and Sørensen (2004) are also presented for comparison. These models are currently used in atmospheric models, such as RACMO (Lenaerts et al., 2012), MAR (Amory et al., 2015), Alpine3D (Lehning et al., 2008) and Meso-NH (Vionnet et al., 2014), to estimate snow saltation mass flux. The expressions proposed by Pomeroy and Gray (1990) and Sørensen (2004) are plotted for two limiting values of the impact threshold: obtained with simulation S3, $\sigma_d = 100$ μm (non-cohesive bed) and with simulation S4, $\phi = 5{\times}10^{-9}$ J. As previously explained, in this work, the impact threshold is assumed equal to the equilibrium friction velocity at the lowest value of u_* that was studied ($u_* = 0.4$ m s^{-1}). The results obtained with the model developed by Doorschot and Lehning (2002) are derived considering a lognormal bed size distribution with $\langle d \rangle = 200$ μm and $\sigma_d = 100$ μm.

The simulation results indicate that Q varies significantly with the cohesion energy. In general, it decreases with ϕ for lower friction velocities and increases with ϕ for greater values of u_*. This is due to the reduction of particle mass flux close to the surface and to its increase at higher elevations as cohesion energy increases (Figure 2j). At low friction velocities ($u_* = 0.4$ m s^{-1}), the reduction of particle mass flux close to the surface prevails, while at greater u_*, the rise in mass flux at higher elevations becomes more significant, leading to a global growth of the integrated mass flux. A better agreement between the expression proposed by Sørensen (2004), using the parameters proposed by Vionnet et al. (2014), and the simulation results is obtained when interparticle cohesion and a lognormal size distribution are considered. This is, when considering a more realistic snow bed. Nonetheless, greater values for Q are predicted with $Q_{S\o}$. An overestimation of the integrated mass flux in saltation is consistent with the overestimation of blowing snow particles obtained by Vionnet et al. (2014). The effect of the impact threshold on $Q_{S\o}$ is mainly visible at lower friction velocities. At $u_* = 0.4$ m s^{-1}, the adjustment of the impact threshold improves the agreement between model and simulation results obtained with different values for cohesion energy. The results obtained with the numerical model of Doorschot and Lehning (2002) agree well with the simulation results obtained with mixed-sized and cohesionless grains or $\phi = 10^{-10}$ J, over the whole range

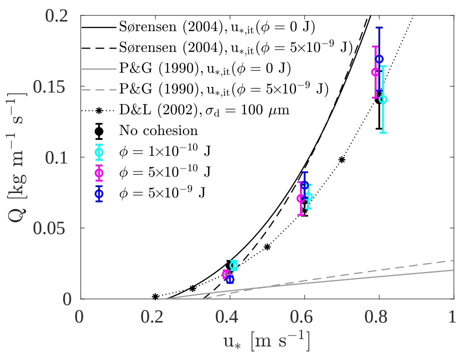

Figure 10. Integrated mass flux obtained with simulations S4 for u_* equal to 0.4, 0.6 and 0.8 m s^{-1}. Results from simulations S3 obtained with the same size distribution and u_* are also presented for comparison. To improve readability, some data points are slightly shifted in the u_* axis. The error bar is twice the standard deviation of the results. The expressions proposed by Sørensen (2004) and Pomeroy and Gray (1990) (P&G) are plotted for comparison considering different values of the impact threshold. The results from Doorschot and Lehning (2002) (D&L) are obtained for a bed characterized by a lognormal distribution with $\langle d \rangle = 200$ μm and $\sigma_d = 100$ μm.

of the studied friction velocities. Even though a good agreement is also obtained over a bed of uniform grains for $u_* < 0.6$ m s^{-1} (Figure 5b), the effect of mean grain diameter and bed heterogeneity on the integrated mass flux predicted by Doorschot and Lehning (2002) is not consistent with the evolution obtained by the present model (Figure 7). The expression proposed by Pomeroy and Gray (1990) considerably underestimates the integrated mass flux in comparison with the simulation results and remaining models, independently of the assumed values for the impact threshold. The underestimation of the saltation mass flux might be one of the causes for the underestimation of blowing snow mass flux obtained by Amory et al. (2015).

5 Conclusions

The modeling of snow saltation is particularly challenging due to the metamorphic nature of snow. Depending on the meteorological conditions, snow grains can have multiple shapes and sizes and form interparticle ice bonds between them. During snow transport, the interparticle bonds break and snow particles shape and size change due to fragmentation and sublimation. However, snow saltation models used in mesoscale models generally neglect these particularities, leading to uncertainties in the estimated mass flux that are difficult to quantify. In this work, an LES-based model coupled with state-of-the-art splash functions is used to simulate the complex particle-wind-bed interactions. This approach allows the modeling of steady state saltation over a variety of bed types and the analysis of the effect of grain size and interparticle cohesion on saltation dynamics.

The numerical model is able to simulate the main saltation characteristics observed in previous models and experiments: the focus point in the average streamwise wind profiles, an average streamwise particle speed close to the surface invariant with respect to the friction velocity, the exponential decay of particle mass flux with increasing height, and the scaling of the integrated mass flux with the square of the friction velocity. Moreover, as expected, for friction velocities sufficiently greater than the fluid threshold, the resulting steady state is characterized by a dynamic equilibrium between splash and deposition. Over mixed-sized beds, different particle size distributions are obtained depending on the distance to the snow surface, as expected when transition from saltation to suspension occurs.

The relative importance of snow bed characteristics on saltation dynamics is analyzed by varying the particle size distribution and interparticle bond strength in a systematic way. Bed characteristics, as grain size and interparticle cohesion, significantly influence saltation dynamics, in particular, particle speed, surface friction velocity and integrated mass flux. Particle speed close to the surface is approximately invariant with respect to the friction velocity for all beds that were considered; however, it varies with the bed type. This is relevant for the development of simple saltation models, which are usually based on an assumption for the near surface particle speed. The average surface friction velocity during steady state saltation, defined here as the equilibrium friction velocity, increases for greater values of the mean grain diameter, standard deviation of the size distribution and interparticle cohesion. The equilibrium friction velocity is tightly correlated with the impact threshold, which is an important parameter to estimate saltation mass flux. Over uniform beds, a negligible variation of the integrated mass flux with particle size is obtained for particles ranging between 200 and 400 μm. When considering a mixed-sized bed characterized by a lognormal distribution, an increase in the integrated mass flux is seen due to an average increase in particle speed and concentration. The results presented highlight that the integrated mass flux over mixed-sized beds can be hardly reproduced by an equally-sized bed with a representative mean diameter - a tempting assumption in simple saltation models. The integrated mass flux also varies with interparticle cohesion, but in a non-monotonous way: it decreases with the strength of interparticle bonds for lower friction velocities and it increases for higher friction velocities. Overall, greater values of cohesion lead to a reduction in the number of particles aloft which, at high wind speeds, is balanced by an increase in particle speed. In general, the greater the friction velocity, the greater the effect of bed properties on saltation characteristics. High wind speed events might be rare in some regions. However, they are responsible for major modifications of the snow cover.

The agreement between simulation results and the saltation models typically used in large scale atmospheric models depends on the bed characteristics. For specific bed types, a relatively good agreement can be obtained with the models of Sørensen (2004), using the parameters proposed by Vionnet et al. (2014), and Doorschot and Lehning (2002). However, these models either consider fixed parameters, which are not adjustable to the snow type, or predict a different variation of the integrated mass flux with the mean grain size and bed heterogeneity. A systematic underestimation and overestimation of the integrated mass flux is obtained with the expression proposed by Pomeroy and Gray (1990) and Sørensen (2004), respectively. This might partly justify the underestimation and overestimation of blowing snow mass flux presented, respectively, by Amory et al. (2015) and Vionnet et al. (2014).

Further efforts must be made to fully model the effect of bed characteristics on snow saltation. For example, interparticle cohesion is also expected to influence particle ejection velocity during splash and the fluid threshold for the onset of aerodynamic entrainment (Comola et al., 2021). Moreover, the strength of interparticle bonds between grains that did not leave the surface and between those that failed to rebound might not be the same. From the experimental work side, a correlation between interparticle cohesion and meteorological conditions or measurable snow properties like snow density or snow hardness is still needed. In addition, exhaustive direct comparisons between simulation results and experimental measurements of snow saltation must be performed to complete model validation. In order to better access the model inner parameters, further studies of the splash process over natural snow beds are required, as well as detailed field measurements characterizing both the wind speed, the snow bed and the particles in saltation.

Simple and computationally inexpensive saltation models are much needed in mesoscale models. However, the in depth study of snow saltation is necessary to fully understand the implications of the simplifying assumptions that are used and to estimate the errors they might introduce. This article shows the capabilities of an LES-based model to simulate snow saltation, presents the effect of bed properties on saltation dynamics and motivates further studies in this field. It highlights the limitations of the snow saltation models currently employed in mesoscale models and the need for improved ones that take into account the effect of snow surface characteristics. Without accurate estimations for the mass flux in saltation, climatological models do not reasonably estimate blowing snow transport and sublimation. Hence, their effect on large scale mass and energy balances is highly compromised.

Acknowledgments

Pedro Cabral is acknowledged for the numerous discussions regarding the results and the in-depth revision of the text. His contribution has greatly improved the clarity of the manuscript. The authors acknowledge the Swiss National Science Foundation (SNSF) for the financial support (projects number 179130 and P2ELP2_178219) and the Swiss National Supercomputing Centre (CSCS) for providing the computational resources (projects s873, s938 and s1031). The results of the simulations are available at https://enacshare.epfl.ch/djzTaD3YGc9HBkdqA2MCt in csv format. The results will be uploaded to the repository www.envidat.ch before acceptance.

References

Agosta, C., Amory, C., Kittel, C., Orsi, A., Favier, V., Gallée, H., . . . Fettweis, X. (2019). Estimation of the Antarctic surface mass balance using the regional climate model MAR (1979–2015) and identification of dominant processes. *The Cryosphere*, *13*(1), 281–296.

Albertson, J. D., & Parlange, M. B. (1999). Natural integration of scalar fuxes from complex terrain. *Advances in Water Resources*, *23*, 239–252.

Almeida, M. P., Andrade, J. S., & Herrmann, H. J. (2006). Aeolian Transport Layer. *Physical Review Letters*, *96*(1), 018001. (Publisher: American Physical Society)

Ammi, M., Oger, L., Beladjine, D., & Valance, A. (2009). Three-dimensional analysis of the collision process of a bead on a granular packing. *Physical Review E : Statistical, Nonlinear, and Soft Matter Physics*, *79*, 021305. (Publisher: American Physical Society)

Amory, C., Trouvilliez, A., Gallée, H., Favier, V., Naaim-Bouvet, F., Genthon, C., . . . Bellot, H. (2015). Comparison between observed and simulated aeolian snow mass fluxes in Adélie Land, East Antarctica. *The Cryosphere*, *9*(4), 1373–1383.

Anderson, R. S., & Haff, P. K. (1988). Simulation of Eolian Saltation. *Science*, *241*(4867), 820–823.

Anderson, R. S., & Haff, P. K. (1991). Wind modification and bed response during saltation of sand in air. In O. E. Barndorff-Nielsen & B. B. Willetts (Eds.), *Aeolian grain transport 1* (pp. 21–51). Springer Vienna.

Anderson, R. S., & Hallet, B. (1986). Sediment transport by wind: Toward a general model. *GSA Bulletin*, *97*(5), 523–535.

Bagnold, R. A. (1941). *The physics of blown sand and desert dunes.* Dover Publications.

Bou-Zeid, E., Meneveau, C., & Parlange, M. (2005). A scale-dependent Lagrangian dynamic model for large eddy simulation of complex turbulent flows. *Physics of Fluids*, *17*(2), 025105.

Canuto, C., Hussaini, M. Y., Quarteroni, A., & Zang, T. A. (1988). *Spectral Methods in Fluid Dynamics.* Springer-Verlag Berlin Heidelberg.

Chepil, W. S. (1959). Equilibrium of Soil Grains at the Threshold of Movement by Wind. *Soil Science Society of America*, *23*(6), 422–428.

Clift, R., Grace, J., Weber, M., & Weber, M. (1978). *Bubbles, drops, and particles.* Academic Press.

Clifton, A., & Lehning, M. (2008). Improvement and validation of a snow saltation model using wind tunnel measurements. *Earth Surface Processes and Landforms*, *33*(14), 2156–2173.

Clifton, A., Rüedi, J.-D., & Lehning, M. (2006). Snow saltation threshold measurements in a drifting-snow wind tunnel. *Journal of Glaciology*, *52*(179), 585–596. (Publisher: Cambridge University Press)

Colbeck, S. (1986). Statistics of coarsening in water-saturated snow. *Acta Metallurgica*, *34*(3), 347–352.

Comola, F. (2017). *Stochastic modeling of snow transport and hydrologic response in alpine terrain* (Unpublished doctoral dissertation). Ecole Polytechnique Fédérale de Lausanne, Lausanne, Switzerland.

Comola, F., Gaume, J., Kok, J. F., & Lehning, M. (2019). Cohesion-Induced Enhancement of Aeolian Saltation. *Geophysical Research Letters*, *46*(10), 5566–5574.

Comola, F., Giometto, M. G., Salesky, S. T., Parlange, M. B., & Lehning, M. (2019). Preferential deposition of snow and dust over hills: Governing processes and relevant scales. *Journal of Geophysical Research: Atmospheres*, *124*(14), 7951–7974.

Comola, F., Kok, J. F., Gaume, J., Paterna, E., & Lehning, M. (2017). Fragmentation of wind-blown snow crystals. *Geophysical Research Letters*, *44*(9), 4195–4203.

Comola, F., Kok, J. F., Lora, J. M., Cohanim, K., Yu, X., He, C., … Turney, F. (2021). Intermittent saltation drives Mars-like aeolian activity on Titan. *EarthArXiv*. doi: 10.31223/X52G7H

Comola, F., & Lehning, M. (2017). Energy- and momentum-conserving model of splash entrainment in sand and snow saltation. *Geophysical Research Letters*, *44*(3), 1601–1609.

Diebold, M., Higgins, C., Fang, J., Bechmann, A., & Parlange, M. B. (2013). Flow over Hills: A Large-Eddy Simulation of the Bolund Case. *Boundary-Layer Meteorology*, *148*(1), 177–194.

Dong, Z., Liu, X., Wang, H., & Wang, X. (2003). Aeolian sand transport: a wind tunnel model. *Sedimentary Geology*, *161*(1), 71–83.

Doorschot, J. J. J., & Lehning, M. (2002). Equilibrium Saltation: Mass Fluxes, Aerodynamic Entrainment, and Dependence on Grain Properties. *Boundary-Layer Meteorology*, *104*(1), 111–130.

Dupont, S., Bergametti, G., Marticorena, B., & Simoëns, S. (2013). Modeling saltation intermittency. *Journal of Geophysical Research: Atmospheres*, *118*(13), 7109–7128.

Durán, O., Andreotti, B., & Claudin, P. (2012). Numerical simulation of turbulent sediment transport, from bed load to saltation. *Physics of Fluids*, *24*(10), 103306. (Publisher: American Institute of Physics)

Durán, O., Claudin, P., & Andreotti, B. (2011). On aeolian transport: Grain-scale interactions, dynamical mechanisms and scaling laws. *Aeolian Research*, *3*(3), 243–270.

Gauer, P. (2001). Numerical modeling of blowing and drifting snow in Alpine terrain. *Journal of Glaciology*, *47*(156), 97–110. (Publisher: Cambridge University Press)

Giometto, M. G., Christen, A., Egli, P. E., Schmid, M. F., Tooke, R. T., Coops, N. C., & Parlange, M. B. (2017). Effects of trees on mean wind, turbulence and momentum exchange within and above a real urban environment. *Advances in Water Resources*, *106*, 154–168.

Giometto, M. G., Christen, A., Meneveau, C., Fang, J., Krafczyk, M., & Parlange, M. B. (2016). Spatial Characteristics of Roughness Sublayer Mean Flow and Turbulence Over a Realistic Urban Surface. *Boundary-Layer Meteorology*, *160*(3), 425–452.

Gordon, M., Savelyev, S., & Taylor, P. A. (2009). Measurements of blowing snow, part II: Mass and number density profiles and saltation height at Franklin Bay, NWT, Canada. *Cold Regions Science and Technology*, *55*(1), 75–85.

Groot Zwaaftink, C. D., Diebold, M., Horender, S., Overney, J., Lieberherr, G., Parlange, M. B., & Lehning, M. (2014). Modelling Small-Scale Drifting Snow with a Lagrangian Stochastic Model Based on Large-Eddy Simulations. *Boundary-Layer Meteorology*, *153*(1), 117–139.

Ho, T. D., Valance, A., Dupont, P., & Ould El Moctar, A. (2011). Scaling Laws in Aeolian Sand Transport. *Physical Review Letters*, *106*(9), 094501.

Huang, N., Zhang, Y., & D'Adamo, R. (2007). A model of the trajectories and midair collision probabilities of sand particles in a steady state saltation cloud. *Journal of Geophysical Research: Atmospheres*, *112*(D8).

Kok, J. F., Parteli, E. J. R., Michaels, T. I., & Karam, D. B. (2012). The physics of wind-blown sand and dust. *Reports on Progress in Physics*, *75*(10), 106901.

Kok, J. F., & Renno, N. O. (2006). Enhancement of the emission of mineral dust aerosols by electric forces. *Geophysical Research Letters*, *33*(19).

Kok, J. F., & Renno, N. O. (2008). Electrostatics in Wind-Blown Sand. *Physical Review Letters*, *100*(1), 014501.

Kok, J. F., & Renno, N. O. (2009). A comprehensive numerical model of steady state saltation (COMSALT). *Journal of Geophysical Research: Atmospheres*, *114*(D17).

Lehning, M., Doorschot, J., & Bartelt, P. (2000). A snowdrift index based on SNOWPACK model calculations. *Annals of Glaciology*, *31*, 382–386. (Publisher: Cambridge University Press)

Lehning, M., Löwe, H., Ryser, M., & Raderschall, N. (2008). Inhomogeneous precipitation distribution and snow transport in steep terrain. *Water Resources Research*, *44*(7).

Lenaerts, J. T. M., van den Broeke, M. R., Déry, S. J., van Meijgaard, E., van de Berg, W. J., Palm, S. P., & Sanz Rodrigo, J. (2012). Modeling drifting snow in Antarctica with a regional climate model: 1. Methods and model evaluation. *Journal of Geophysical Research: Atmospheres*, *117*(D5).

Lämmel, M., Dzikowski, K., Kroy, K., Oger, L., & Valance, A. (2017). Grain-scale modeling and splash parametrization for aeolian sand transport. *Physical Review E*, *95*(2), 022902. (Publisher: American Physical Society)

Martin, R. L., & Kok, J. F. (2017). Wind-invariant saltation heights imply linear scaling of aeolian saltation flux with shear stress. *Science Advances*, *3*(6), e1602569.

Martin, R. L., & Kok, J. F. (2019). Size-Independent Susceptibility to Transport in Aeolian Saltation. *Journal of Geophysical Research: Earth Surface*, *124*(7), 1658–1674.

Maxey, M. R., & Riley, J. J. (1983). Equation of motion for a small rigid sphere in a nonuniform flow. *The Physics of Fluids*, *26*(4), 883–889. (Publisher: American Institute of Physics)

McEwan, I. K., & Willetts, B. B. (1991). Numerical model of the saltation cloud. In O. E. Barndorff-Nielsen & B. B. Willetts (Eds.), *Aeolian grain transport 1* (pp. 53–66). Springer Vienna.

Munters, W., Meneveau, C., & Meyers, J. (2016). Shifted periodic boundary conditions for simulations of wall-bounded turbulent flows. *Physics of Fluids*, *28*(2), 025112. (Publisher: American Institute of Physics)

Nalpanis, P., Hunt, J. C. R., & Barrett, C. F. (1993). Saltating particles over flat beds. *Journal of Fluid Mechanics*, *251*, 661–685. (Publisher: Cambridge University Press)

Nemoto, M., & Nishimura, K. (2004). Numerical simulation of snow saltation and suspension in a turbulent boundary layer. *Journal of Geophysical Research: Atmospheres*, *109*(D18).

Nishimura, K., Yokoyama, C., Ito, Y., Nemoto, M., Naaim-Bouvet, F., Bellot, H., & Fujita, K. (2014). Snow particle speeds in drifting snow: Snow particle speeds in drifting snow. *Journal of Geophysical Research: Atmospheres*, *119*(16), 9901–9913.

Okaze, T., Niiya, H., & Nishimura, K. (2018). Development of a large-eddy simulation coupled with Lagrangian snow transport model. *Journal of Wind Engineering and Industrial Aerodynamics*, *183*, 35–43.

Owen, P. R. (1964). Saltation of uniform grains in air. *Journal of Fluid Mechanics*, *20*(2), 225–242.

Palm, S. P., Kayetha, V., Yang, Y., & Pauly, R. (2017). Blowing snow sublimation and transport over Antarctica from 11 years of CALIPSO observations. *The Cryosphere*, *11*(6), 2555–2569.

Pomeroy, J. W., & Gray, D. M. (1990). Saltation of snow. *Water Resources Research*, *26*(7), 1583–1594.

Pähtz, T., Clark, A. H., Valyrakis, M., & Durán, O. (2020). The Physics of Sediment Transport Initiation, Cessation, and Entrainment Across Aeolian and Fluvial Environments. *Reviews of Geophysics*, *58*(1), e2019RG000679.

Pähtz, T., Omeradžić, A., Carneiro, M. V., Araújo, N. A. M., & Herrmann, H. J.

(2015). Discrete Element Method simulations of the saturation of aeolian sand transport. *Geophysical Research Letters*, *42*(6), 2063–2070.

Rice, M. A., Willetts, B. B., & McEwan, I. K. (1995). An experimental study of multiple grain-size ejecta produced by collisions of saltating grains with a flat bed. *Sedimentology*, *42*(4), 695–706.

Rice, M. A., Willetts, B. B., & McEwan, I. K. (1996). Observations of collisions of saltating grains with a granular bed from high-speed cine-film. *Sedimentology*, *43*(1), 21–31.

Schmidt, D. S., Schmidt, R. A., & Dent, J. D. (1998). Electrostatic force on saltating sand. *Journal of Geophysical Research: Atmospheres*, *103*(D8), 8997–9001.

Schmidt, R. A. (1980). Threshold Wind-Speeds and Elastic Impact in Snow Transport. *Journal of Glaciology*, *26*(94), 453–467.

Shao, Y., & Li, A. (1999). Numerical Modelling of Saltation in the Atmospheric Surface Layer. *Boundary-Layer Meteorology*, *91*(2), 199–225.

Shao, Y., & Lu, H. (2000). A simple expression for wind erosion threshold friction velocity. *Journal of Geophysical Research: Atmospheres*, *105*(D17), 22437–22443.

Shao, Y., Raupach, M. R., & Findlater, P. A. (1993). Effect of saltation bombardment on the entrainment of dust by wind. *Journal of Geophysical Research: Atmospheres*, *98*(D7), 12719–12726.

Sharma, V., Comola, F., & Lehning, M. (2018). On the suitability of the Thorpe–Mason model for calculating sublimation of saltating snow. *The Cryosphere*, *12*(11), 3499–3509.

Sharma, V., Parlange, M. B., & Calaf, M. (2017). Perturbations to the Spatial and Temporal Characteristics of the Diurnally-Varying Atmospheric Boundary Layer Due to an Extensive Wind Farm. *Boundary-Layer Meteorology*, *162*(2), 255–282.

Sørensen, M. (1991). An analytic model of wind-blown sand transport. In O. E. Barndorff-Nielsen & B. B. Willetts (Eds.), *Aeolian grain transport 1* (pp. 67–81). Springer Vienna.

Sørensen, M. (2004). On the rate of aeolian sand transport. *Geomorphology*, *59*(1), 53–62.

Ungar, J. E., & Haff, P. K. (1987). Steady state saltation in air. *Sedimentology*, *34*(2), 289–299.

Van Wessem, J. M., van de Berg, W. J., Noël, B. P. Y., van Meijgaard, E., Amory, C., Birnbaum, G., … van den Broeke, M. R. (2018). Modelling the climate and surface mass balance of polar ice sheets using RACMO2 – Part 2: Antarctica (1979–2016). *The Cryosphere*, *12*(4), 1479–1498.

Vionnet, V., Martin, E., Masson, V., Guyomarc'h, G., Naaim-Bouvet, F., Prokop, A., … Lac, C. (2014). Simulation of wind-induced snow transport and sublimation in alpine terrain using a fully coupled snowpack/atmosphere model. *The Cryosphere*, *8*(2), 395–415.

Walter, B., Horender, S., Voegeli, C., & Lehning, M. (2014). Experimental assessment of Owen's second hypothesis on surface shear stress induced by a fluid during sediment saltation. *Geophysical Research Letters*, *41*(17), 6298–6305.

Wang, D., Wang, Y., Yang, B., Zhang, W., & Lancaster, N. (2008). Statistical analysis of sand grain/bed collision process recorded by high-speed digital camera. *Sedimentology*, *55*(2), 461–470.

Wang, Z., Huang, N., & Pähtz, T. (2019). The Effect of Turbulence on Drifting Snow Sublimation. *Geophysical Research Letters*, *46*(20), 11568–11575.

Xing, M., & He, C. (2013). 3D ejection behavior of different sized particles in the grain-bed collision process. *Geomorphology*, *187*, 94–100.